Background Limited Quantum Superconducting Detector for Submillimeter Wavelengths

Gregory Gol'tsman, Alexei Semenov*, Konstantin Smirnov, and Boris Voronov

State Pedagogical University of Moscow, 119891 Moscow, Russia
** DLR Institute of Space Sensor Technology and Planetary Exploration, 12489 Berlin, Germany*

ABSTRACT

We propose a concept of the background-limited detector for submillimeter radioastronomy that will have the noise equivalent power $\approx 10^{-21}$ W $Hz^{-1/2}$ when operated at 0.3 K and exposed to thermal background radiation with an equivalent temperature of 4 K. The detector is based upon the superconducting photon counter from Titanium film integrated into a planar logarithmic antenna. The planar layout makes feasible integration of the device in a detector array.

Introduction

Future radioastronomy missions will require detectors, which provide ultimate (background limited) sensitivity in the submillimeter wavelength range even when exposed to relatively weak background radiation. In comparison with different detection regimes, the photon counting regime is by definition the one having ultimate sensitivity. There has been recently proposed [1] a single-photon detection mechanism in a current carrying superconducting film that may become a basement for the development of the novel detector meeting observation requirements. The mechanism of the photon detection is the following. Photon absorbed in the superconducting film creates growing normal spot that forces the current to bypass the absorption site. When the current density in the superconducting areas reaches the critical value, the film switches into the resistive state and generates the voltage pulse. Operation of NbN photon counter [2] has been recently demonstrated. Both theoretical estimate [1] and extrapolation of experimental data [3] show, however, that the NbN counter will have a cutoff wavelength for the single photon detection regime of about 10 μm. Implementation of low-transition-temperature superconducting materials and subkelvin operation temperatures will shift the cutoff wavelength towards submillimeter range. Here we present estimates of the performance of the Ti based quantum detector for radiastronomy and first results of device manufacturing and characterization.

E-mail addresses: goltsman00@mail.ru ; Alexei.Semenov@dlr.de

Operation Principle of the Superconducting Quantum Detector

The key element of the quantum detector is a superconducting film patterned into a narrow strip, which is biased along its length with the current slightly less than the critical current at the operation temperature. The film thickness should be comparable or smaller than its width. In order to have significant coupling with radiation, the strip should be integrated into a planar antenna or form the meander-line covering the area larger than squared wavelength. Once a photon is absorbed at some point in the strip, it produces a high-energy electron, which then shares its energy with low-energy electrons by means of electron-electron and electron phonon interaction. The process is commonly called multiplication, since the number of low-energy unpaired electrons grows in time. The maximal number of additional electrons appearing in the film per one absorbed photon is referred as quantum yield or quantum efficiency. This figure increases in proportion to the ratio of the quantum energy and the superconducting energy gap. At any point in the film, the concentration of unpaired electrons increases due to multiplication and decreases due to out-diffusion. Once their concentration has exceeded the value specific for the normal state at $T = T_C$ (T_C is the superconducting transition temperatire), unpaired electrons suppress the energy gap and destroy superconductivity. The normal spot appears at a position where the photon has been absorbed. This forces the supercurrent to flow around the spot through still superconducting portion of the film. With the increase of the spot size the current density in the superconducting sidewalks increases and reaches the critical value. At this very moment the resistive "membrane" is formed across the cross-section area of the film, giving rise to the voltage pulse with the magnitude proportional to the bias current. Thus, the response appears due to collaborative effect of the bias current and the growing normal domain.

From this simple description one can see that the ability of the detector to register a single photon is the trade-off between the film width, the bias current, and the photon energy. The minimal film width is restricted to approximately 100 nm by available structuring technology. The magnitude of the bias current is limited by thermal fluctuations and/or by fluctuations of the superconducting phase. To achieve the background limited performance; fluctuations of the critical current should be less than the difference between the critical current and the bias current. In this case, the detector noise equivalent power is limited by phase fluctuations, which produce voltage pulses (dark counts) indistinguishable from those resulted from absorbed photons.

Since the quantum efficiency drops with the increase of the wavelength, there is a cutoff wavelength for the above described detection mechanism. Low energy photon can not produce the concentration of unpaired electrons, which is sufficiently large in order to suppress superconductivity. For NbN quantum detector, the cutoff occurs in the near infrared spectral range. The quantum efficiency, however, turns to be larger in a superconducting material with smaller transition temperature, because the superconducting energy gap decreases with the transition temperature. The normal-state concentration of the electrons, which should be reached during multiplication in order to destroy superconductivity, also decreases with the transition temperature. Thus, the use of a material with smaller transition temperature will shift the cutoff towards longer

wavelength. Provided a sufficiently high optical coupling, such a detector may compete with traditional background limited thermal detectors in the submillimeter wavelength range.

Quantum Detector from Titanium: Performance simulation

We simulate major figures of merit for the detector from Ti superconducting film making use of the model described in Ref. 1. We do not know some of required film parameters. Although this increases uncertainty of the estimate, we believe that our results are quite realistic. We took the density of states for bulk Titanium [4] and the Bardeen-Cooper-Schrieffer (BCS) energy gap. The electron-electron interaction time at the Fermi level was calculated in the extreme dirty limit [5] using the expression

$$\tau_{ee}^{-1} = \frac{k_B}{4\hbar R_q} R_S T_C \ln\left(2\frac{R_q}{R_S}\right), \qquad (1)$$

where $Rq = h/(4e^2) = 6.47$ kΩ is the resistance quanta and R_S is the sheet resistance of our films. Electron diffusivity was concluded from the Lorentz number and the value [4] of the Sommerfeld constant $6.8 \cdot 10^{-4}$ J cm^{-3}K^{-2} for bulk material. The Table below contains the material parameters, which we used for simulation.

Table 1 Material parameters of titanium films.

Transition temperature	Energy gap at T = 0	Electron-electron interaction time	Electron density of states	Electron diffusivity
0.6 K	1.06 K	400 psec	$6.8 \cdot 10^{24}$ m^{-3}K^{-1}	0.4 cm^{2}sec^{-1}

The cutoff wavelength for Ti and NbN films at different bias currents and strip widths is shown in Fig. 1 for the operation temperature 0.5 T_C. Material parameters of NbN films were taken from [1]. The film thickness was assumed 5 nm in both cases. According to our estimate, a detector from Titanium should provide at least an order of magnitude larger cutoff wavelength than NbN photon counters.

Photon counting regime brings peculiarities into the signal processing that do not allow for direct comparison of thermal detectors (bolometers) and quantum detectors in terms of the noise equivalent power. We examine here main performance figures of the Ti quantum detector whereas a detailed analysis of the counting statistics will be published elsewhere. The maximum intensity of the narrow-band background radiation, which the device can sustained while keeping the photon counting capability, is given by

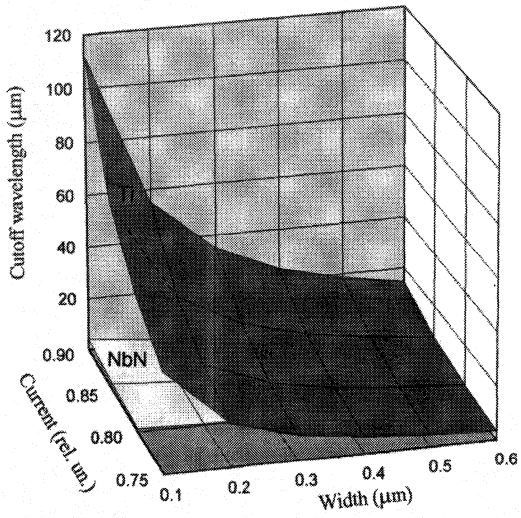

FIG.1 Cutoff wavelength for NbN and Ti quantum detectors. Bias current is plotted in units of the critical current at the operation temperature.

the expression $\eta h\nu/\Delta t$ where $\Delta t = 0.2\tau_{ee}$ is the duration of the response voltage transient, η is the optical coupling efficiency, and $h\nu$ is the quantum energy. Assuming 100-μm cutoff wavelength and typical optical coupling –10 dB, which has been demonstrated [6] for an integrated antenna in this wavelength range, we obtain an upper limit of $2\cdot10^{-10}$ W for the background radiation power. For a diffraction limited antenna with the 6-mm effective aperture [6], this power corresponds to the 42-K thermal background and results in the background limited noise equivalent power (NEP) $1.2\cdot10^{-15}$ W $Hz^{-1/2}$. The smallest power, at which the detector still has background limited sensitivity, is determined by the dark count rate. Provided that the bias current is sufficiently small in order to prevent switching of the film into the normal state due to thermal fluctuations, the origin of dark counts is the 2π-slippage of the superconducting phase leading to voltage pulses at the device outer contacts. According to [7], the probability of the slippage depends on the reciprocal phase relaxation time (Ginzburg-Landau relaxation time), superconducting condensation energy, and the bias current. Additionally taking into account the dependence of the condensation energy on the bias current, we estimated for the 100-nm wide Ti film biased with the current 0.9 I_C (I_C is the critical current) at $T = 0.5\ T_C$ the mean dark count rate $\approx 10^2$ sec^{-1}. For 100-μm cutoff wavelength this corresponds to the input radiation power $1.7\cdot10^{-18}$ W. The same count rate would produce quanta of the thermal background with a temperature of 6.3 K. The background limited NEP decreases in this regime to $5\cdot10^{-20}$ W $Hz^{-1/2}$. Thus, the photon detector is expected to provide background-limited performance within the dynamic range, which approaches eight orders of magnitude. Further decrease of the background radiation intensity does not lead to a better performance, since NEP is limited by dark counts. For a photon counter, the effective signal integration bandwidth equals the reciprocal chopping frequency. Since for a statistical ensemble of 10^2 events the apparent mean square deviation does not

practically differ from the deviation for an infinite number of events, one would need few second observation time at the chopping frequency 1 Hz in order to realize the best noise equivalent power.

In order to compare our detector with alternative hot-electron bolometer detectors [8,9], we specify also the noise equivalent power transformed to the device input. Setting the optical coupling $\eta = 1$, we obtain the NEP of the detector itself $5 \cdot 10^{-21}$ W Hz$^{-1/2}$. The smallest power providing background limited regime will be $1.7 \cdot 10^{-19}$ W, which corresponds to the background temperature of 4 K for the 100-μm cutoff wavelength. It is worth noting that the spectral cutoff of our detector plays the role of a built-in filter that effectively decreases the background radiation intensity and, correspondingly, the noise equivalent power. Without the cutoff, the full power absorbed by our detector from 4 K-background would be $2 \cdot 10^{-15}$ W, which is close to the saturation level predicted [9] for hot-electron-bolometer detectors.

Manufacturing and characterization of the detector

Our detector is a planar device fabricated on a silicon substrate. The detector represents a narrow bridge pattern from Ti film. The bridge connects inner terminals of a logarithmic spiral antenna structured from gold film on the same substrate. Fabrication process included several deposition and lithographic stages. At the first stage the inner part of the spiral antenna was evaporated by electron-beam sputtering through the mask made by lift-off electron-beam lithography. Thickness of the inner spiral was 100 nm. The gap between antenna terminals had the width of 0.2 μm. At the second stage Ti film was deposited through the mask made by electron-beam lithography. The mask opened a rectangular 0.2-μm width and 2-μm long window that overlapped the gap between antenna terminals. The film was deposited by means of dc reactive magnetron sputtering of the pure Ti target in argon atmosphere at a pressure of 10^{-2} mbar. The length of the bridge, i.e. the active area of the detector, was 0.2 μm as determined by the gap between the antenna terminals. The edges of the Ti strip situated on the gold antenna terminals, providing electrical contact to the active area. Finally, outer part of the spiral antenna and contact pads for wiring the detector were made from 200-nm thick gold film by lift-off UV lithography and thermal evaporation. SEM image in Fig. 2 shows the layout of the central part of the detector.

Detector exhibited a superconducting transition temperature of 0.64 K and 0.53 K for 25 nm and 30 nm thick Ti bridge, respectively. In both cases the width of the superconducting transition was less than 0.02 K. The critical current density $1.5 \cdot 10^{3}$ A cm^{-2} measured at 0.5 T_C was noticeably smaller than the value concluded from the BCS theory. The reason for the discrepancy is not yet clear. We shall mention here that an increase of the critical current density would result in a larger output voltage transient, thus making easier the signal readout. On the other hand, larger bias current would hamper the noise equivalent power because the dark count rate exponentially grows with the bias current.

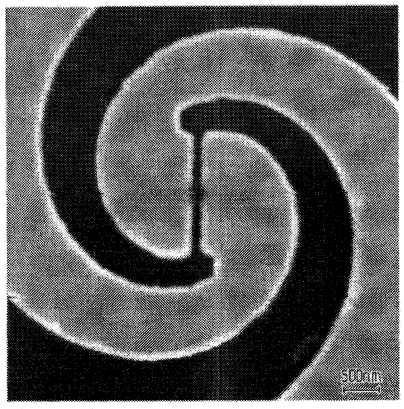

FIG.2 SEM image of the central part of the detector. Ti strip (gray shadow rectangle) bridges the inner terminals of the spiral antenna.

Focal Plane Array and Readout

The planar technology makes integration of our detectors into a detector array relatively simple. An example of possible array architecture is shown in Fig. 3. Detectors are patterned on the rectangular or hexagonal grid on one side of the wafer, which carries an antireflection coating on the irradiation side. The second wafer containing bias lines and SQUID read-out is flip-chipped to the first one carrying detectors. Assuming a single

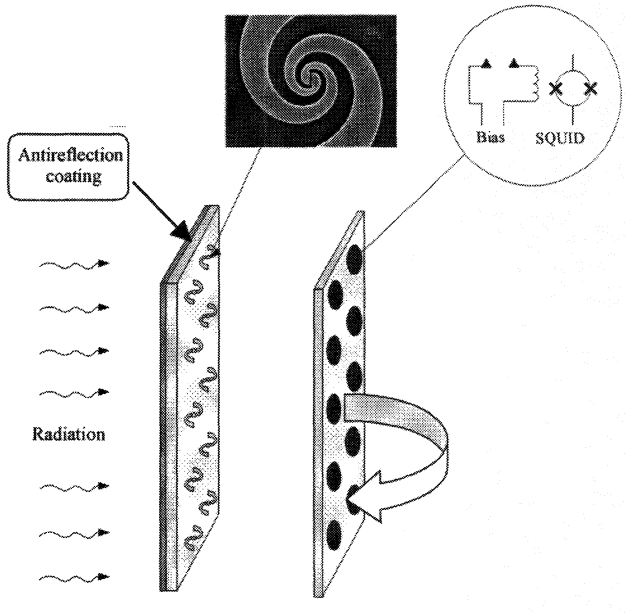

FIG. 3 Focal plane quantum detector array with flip-chip SQUID readout.

pixel with the diffraction limited size, that is ≈ 50 μm for silicon wafer, and the hexagonal grid, we estimate the 5.3 mm radius of the 10^4-pixel array. With the corresponding filling factor of about 0.9, the optical coupling will be mostly determined by the efficiency of individual antennas. However, the array will require an additional lens or mirror to convert its relatively large F-number ≈ 70 into the value of about 10, which is typical for telescopes. Besides the lower dissipated power in comparison to solid state amplifiers, the advantage of the SQUID readout is a larger signal to noise ratio. This is especially important when detectors are biased with the small current resulting in the magnitude of the signal transient below the millivolt level.

Conclusion

We have shown that the novel Ti superconducting quantum detector is a prospective single-pixel element for submillimeter focal plane detector arrays. Our detector offers background limited sensitivity in the range of background intensity much broader than hot-electron bolometers, while its noise equivalent power at a weak background should be comparable or better than NEP projected for hot-electron devices.

References

[1] A.D. Semenov, G.N. Gol'tsman, and A.A. Korneev, "Quantum detection by current carrying superconducting film", *Physica C*, 2001.

[2] G. Gol'tsman, O. Okunev, G. Chulkova, A. Lipatov, A. Dzardanov, K. Smirnov, A. Semenov, B. Voronov, C. Williams, and Roman Sobolewski, "Fabrication and properties of an ultrafast NbN hot-electron single-photon detector", *Applied Superconductivity Conference ASC'2000*, Virginia Beach, VA, September 2000.

[3] A. Verevkin et al., this conference Proceedings.

[4] C.P. Poole, H.A. Farach, R.J. Creswick, *Superconductivity*, Academic Press, New York 1995, ISBN 0-12-561455-1.

[5] B. Altshuler and A. Aronov, *Electron-Electron Interaction in Disordered Systems*, North Holland, Amsterdam 1985.

[6] A.D. Semenov, H.-W. Hübers, J. Schubert, G.N. Gol'tsman, A.I. Elantiev, B.M. Voronov, and E.M. Gershenzon, "Design and performance of the lattice-cooled hot-electron terahertz mixer", *J. Appl. Phys* **88**, 6758 (2000).

[7] D.E. McCumber and B.I. Halperin, "Time scale of intrinsic resistive fluctuations in thin superconducting wires", *Phys. Rev.* **B1**, 1054 (1970).

[8] M.E. Gershenson, D. Gong, T. Sato, B.S. Karasik, W.R. McGrath, and A.V. Sergeev, "Hot-electron direct detectors: towards record sensitivity via disorder-suppressed electron-phonon coupling", *Proc. 11th Int. Symp. on Space Terahertz Technology*, May 1-3, 2000, University of Michigan, Ann Arbor, MI, pp.514-523.

[9] D. Chouvaev, L. Kuzmin, M. Tarasov, Normal-metal hot-eletron microbolometer with on-chip protection by tunnel junctions, Supercond. Sci. Technol. **12**, 985 (1999).